

Chapter 3

Online Assessment of Battery Performance

3.1 Introduction

Accurate estimation of the State-of-Charge (SOC) and State-of-Health (SOH) are of great significance in battery management system due to the requirement of ensuring safe and reliable operation of a Li-ion battery in EVs. For driving purpose, it is essential for the driver to have information about how long the driver can still drive with the present charge in the battery. If the driver does not have the precise information, it will create a lot of inconvenience if the charge gets finished before completion of the ride. Conventional internal combustion engine automobile has a dashboard for fuel gauge that shows the absolute level of fuel remaining in the tank. Similarly, battery SOC corresponds to the amount of energy left inside a battery to power the EVs. For EVs customers it is essential to determine the current remaining available capacity so that driver can recharge or change the battery for traveling. Moreover, another inevitable problem with the battery is that their performance (health) deteriorate gradually with cycling (usage) and calendar life (aging) due to irreversible chemical changes with load variations. With the determination of the current remaining available capacity of the battery, it is also vital to identify battery current maximum available capacity ahead of time so that decision for battery replacement could be made. In the combined equivalent circuit based battery model, the energy balance circuit represents battery degradation with charging and discharging with the help of $R_{s,dis}$ and C_{use} . Battery SOC variation is given by V_{SOC} whose value changes between 0 to 1. The accuracy of SOC estimation depends mainly on the fidelity of the

battery model and the robustness of the estimation techniques. The review related to the estimation of internal battery states identify that estimation can be performed by utilizing conventional, data-driven and model-based methods. The conventional methods are easy to implement, however, they are highly affected by external distributions. Data-driven methods perform well with non-linear and high dimensional models with an ability to predict the internal states accurately by using well-computed training data for all possible operating condition. Generation of a large amount of data is the main drawback of data-driven methods which demands large memory and complex computation. The nonlinear observer has enhanced robustness against the disturbances and improved performance in terms of accuracy, converge speed and computation cost. Nevertheless, the model could deliver inaccurate results if the controller is not properly designed. Adaptive filters are the most favored techniques since they can predict non-linear dynamics states with good precision, high efficiency and less computational cost. As the battery model has been developed to represents the dynamic behavior of the battery, hence, model-based adaptive filters recognized as appropriate battery internal states estimation methods. Different variants of adaptive filters are utilized for estimation of internal battery states. In this work, comparison among the model-based estimation techniques such as Extended Kalman Filter (EKF), Sigma-point Kalman Filter (SPKF) and Particle Filter (PF) for estimation of battery SOC has been performed. The battery model developed in Chapter 2 has been used for analyzing the quality and execution time for the different variant of KF. Model-based estimation methods have been compared regarding their robustness, accuracy and computational time. The voltage response circuit of the combined equivalent battery model primary intended to capture the short-term behavior of the batteries in terms charging and discharging process. Whereas, battery capacity degradation is the much slower chemical reaction. To mismatch in the complexity and time-scale, most battery capacity degradation model are based on pattern analysis of measured data rather than the fundamental process modeling. To determine the general model for capacity degradation empirical equations based models are developed by using curve fitting techniques. With the help of empirical capacity degradation model, the complexity of model tuning can be reduced notably. In this work, two different empirical capacity degradation models have been developed and their effectiveness in analyzed for representing the degradation behavior of the battery. Empirical battery capacity degradation model was developed by curve fitting using capacity degradation data obtained from the life-cycle test. Information about battery current SOH and remaining useful life (RUL) has been determining by using different model-based estimation technique and effectiveness of each method in estimation is analyzed. This chapter deals with the estimation of internal

states of the battery using model-based estimation methods. Problem formulation using a state space model regarding the estimation of internal states of the battery has been defined in Section 3.2. The state space model for estimation of battery SOC is realized using the voltage response circuit developed in Chapter 2. Whereas the state space model for battery SOH estimation is accomplished using the empirical model developed using life-cycle test data. Detail description about process method and estimation techniques has discussed in Section 3.3. Estimation results under different operating conditions are shown in Section 3.4 to authenticate the validity of the proposed methods and conclusion obtained regarding the estimation of SOC and SOH is given in the Section 3.5.

3.2 Problem Formulation for Estimation of Battery Internal States

The model-based adaptive filter methods are designed to estimate internal states of the battery based on the state-space model. The diagnostic models have configured for one-step ahead prediction, which allow recursive estimation of battery states [157]. A general discrete-time state-space model that describes characteristics of the system governed by the non-linear stochastic difference equations are defined as follow [229]:

State Equation

$$x_{k+1} = f(x_k, u_{k+1}, w_k) \quad (3.1)$$

with a measurement

Measurement Equation

$$y_{k+1} = h(x_{k+1}, u_{k+1}, v_{k+1}) \quad (3.2)$$

Here, $x \in \mathbb{R}^n$ represents the n-dimensional unobserved state vector of the system; $y \in \mathbb{R}^m$ represents the m-dimensional output measurement vector ; $u \in \mathbb{R}^{N_u}$ represents the known (measured/deterministic) one-dimensional input vector of the system; random variable $w \sim \mathcal{N}(\bar{w}, \sum_w)$, $\sum_w \in \mathbb{R}^{N_w \times N_w}$ and $v \sim \mathcal{N}(\bar{v}, \sum_v)$, $\sum_v \in \mathbb{R}^{N_v \times N_v}$ represents the Gaussian process-noise and the Gaussian measurement-noise (respectively), describing uncertainty in real system. Both process and measurement noise are assumed to be independent from each other hence they have zero mean value and variance represented by \sum_w and \sum_v respectively. Subscript k with variable indicates the value of that variable at the time t_k where $t_k = t_0 + k\delta$ and δ is the time step. Correspondingly, non-linear function $f(.)$ relates

the state at the previous time step k to the state at current time step $k+1$ and non-linear function $h(\cdot)$ relates the state x_k to the measurement y_k . And the state x of the system has mean \bar{x} and covariance \sum_x .

3.2.1 SOC estimation model

A battery can be modeled as a nonlinear, time-varying system with state variables that describe states. The measurement are typically the voltage, current and temperature. In the previous chapter, the battery model has been expressed by continuous time ordinary differential equations. For the implementation of SoC estimation strategies, the discrete form of battery model has to be utilized. To represent battery model by discrete-time ordinary difference equations, assume sampling time Δt to be small enough such that current can be considered constant over sampling time. The battery model discrete state-space equations describing dynamic effect derived from equation (1.1) and (2.12) can be expressed as:

State Equation

$$\begin{bmatrix} SOC_{k_i+1} \\ V_{RC,k_i+1} \end{bmatrix} = \begin{bmatrix} 1 & 0 \\ 0 & \exp^{\frac{-\Delta t}{R_{1,k_i} C_{1,k_i}}} \end{bmatrix} \begin{bmatrix} SOC_{k_i} \\ V_{RC,k_i} \end{bmatrix} + \begin{bmatrix} -\frac{\Delta t}{Q_n} \\ (1 - \exp^{\frac{-\Delta t}{R_{1,k_i} C_{1,k_i}}}) R_1 \end{bmatrix} (I_{BL,k_i} + w_{k_i}) \quad (3.3)$$

Measurement Equation

$$V_{Bt,k_i+1} = V_{oc}(SOC_{k_i+1}) - I_{BL,k_i+1} R_{0,k_i+1} - V_{RC,k_i+1} + v_{k_i+1} \quad (3.4)$$

Here, k_i refers iteration number, the state vector is $x = [SOC \ V_{RC}]^T$ and the current I_{BL} and terminal voltage V_{Bt}^M as the input and output variables respectively.

3.2.2 Capacity degradation model

Battery aging will reduce the maximum available battery capacity compared to the fresh battery. Battery capacity degradation occurs with repeated charging and discharging of the battery. Prognostic of battery failure can be performed by developing capacity degradation model from life-cycle test data. The capacity degradation model is developed by using life-cycle test datasets for 18650 commercialized (LFP) Li-ion batteries. Four different battery $B_1 - B_4$ has been examined to collect the datasets. The battery

degradation datasets have been adopted from the Center for Advanced Life Cycle Engineering (CALCE) battery research group of the University of Maryland. The life-cycle test has been conducted sequentially by performing multiple charging-discharging cycles under room temperature and repeated until capacity degraded to 80 % of maximum capacity of the unused battery. Using the battery test equipment, firstly the batteries were fully charged at constant current with 1C charging rate (i.e., 1.1A) under standard constant current-constant voltage mode. The batteries have been charged until the battery voltage reaches to 4.2V then current has exponential drop till 0.05A while maintaining batteries voltage at 4.2V. Discharging was carried out at a 1C rate until the batteries voltage reaches 2.5V. The test was run at room temperature which was approximately 25°C. The discharge capacity was recorded after each full charge-discharge process. Data collection will terminate when battery full charge capacity reaches EUL point. The detail specification of the battery is listed in Appendix A. Figure 3.1 shows capacity degradation data obtained from the life-cycle test of four different battery.

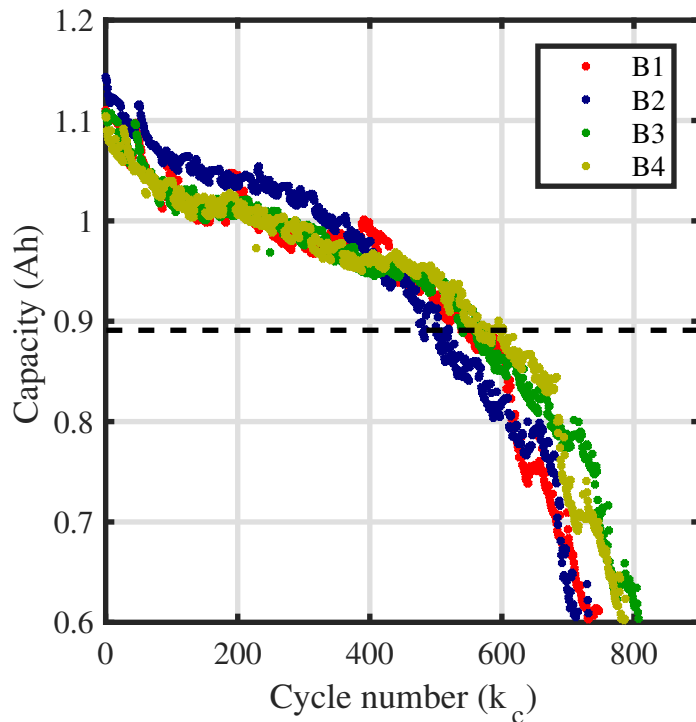


FIGURE 3.1: Capacity data set

Two empirical regression models have been considered to investigated the battery capacity degradation behavior through life-cycle test data. A polynomial and exponential model have been empirically established through fitting of battery degradation data using regression analysis.

Polynomial model

$$Q_{pk_c} = p_1 * k_c^2 + p_2 * k_c + p_3 \quad (3.5)$$

Exponential Model

$$Q_{ek_c} = e_1 * \exp(e_2 * k_c) + e_3 * \exp(e_4 * k_c) \quad (3.6)$$

Where k_c refers the cycle number, parameters of polynomial model and exponential model are represented thorough p_1, p_2, p_3 and e_1, e_2, e_3, e_4 respectively.

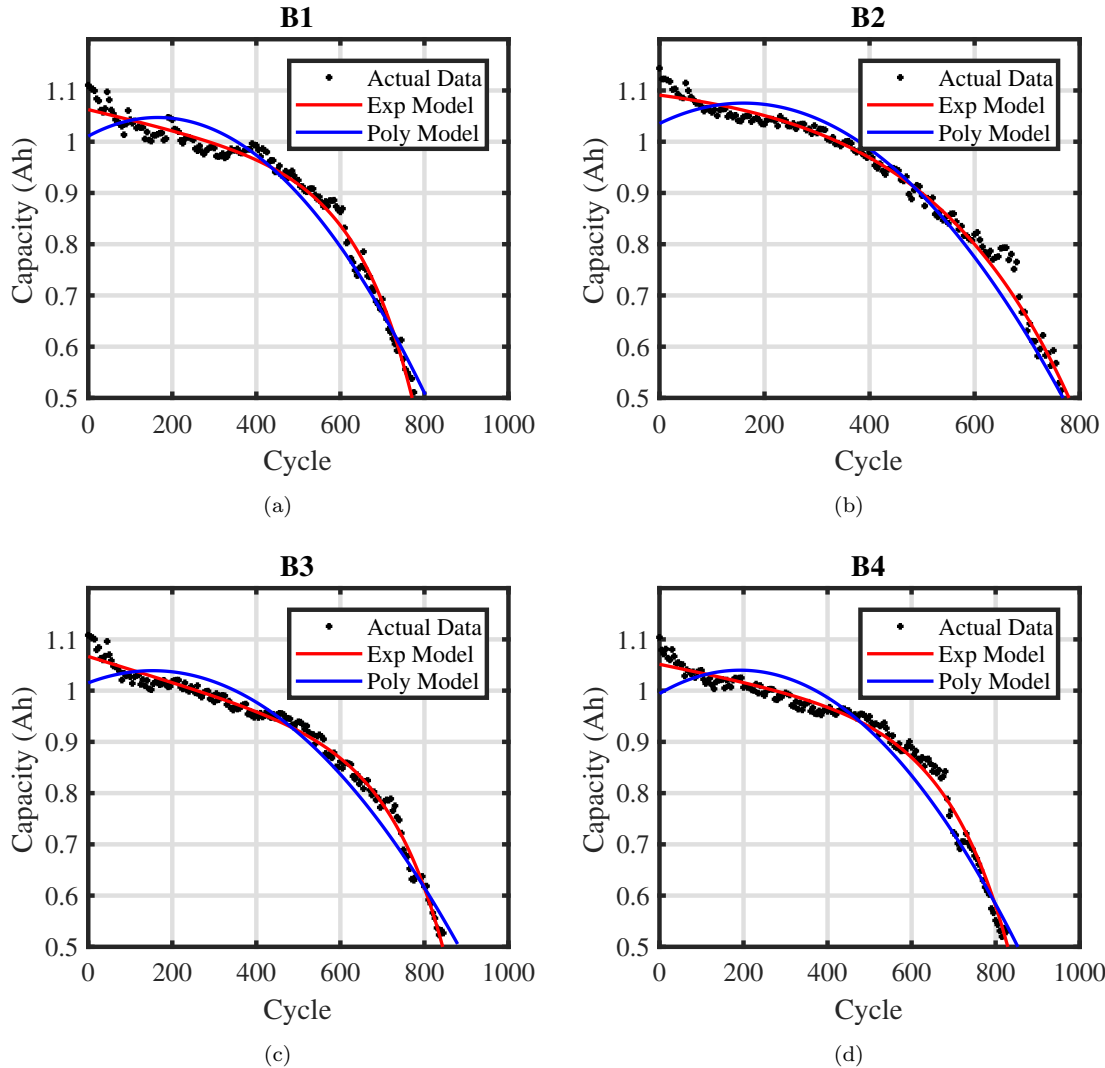


FIGURE 3.2: Curve fitting based on polynomial and exponential model.

To evaluate the goodness-of-fit of given models capacity data over the whole life (up to EUL) was used. Models fitting is performed in MATLAB environment using curve fitting tool. Based on the model's characteristics polynomial model was estimated using linear

least square method while the exponential model was determined using the nonlinear least square method. Aim of both the methods is to minimize the sum of the square of the errors. Figure 3.2 shows curve fitting for battery B1-B4 based on polynomial model and exponential model. Figure 3.2 shows that exponential model fits well with data as compared to polynomial model. Obtained mean parameters value for both polynomial model and exponential model with lower bound and upper bound are shown in Table 3.2. Fitted parameters are calculated with the bound of 95% confidence intervals. With help of lower and upper bound parameters value variance of parameter can also be calculated for further use.

The accuracy of prediction of battery performance and health depends upon the accuracy of the capacity model. Model accuracy and goodness-of-fit of regression can be validated by using two indices the adjusted R-square and RMSE. R_{adj}^2 is modification of R_{square} to compensate for the extra variable included in the model. The best fit is indicated by “1” in R_{adj}^2 and “0” in RMSE. Table 3.1 shows the value of adjusted R-square and RMSE for both exponential and polynomial model. From the table, it can be analyzed that for exponential model the adjusted R^2 is more close to 1 and RMSE is near to 0 compared to the polynomial model. This shows that the exponential model has better global regression performance compare to the polynomial. Hence exponential model is suitable for analysis degradation of battery capacity and predicting RUL.

TABLE 3.1: Goodness-of-fit for polynomial and exponential model

Battery	R^2		RMSE		Adjust R^2	
	Polynomial	Exponential	Polynomial	Exponential	Polynomial	Exponential
B1	0.9430	0.9861	0.0392	0.0194	0.9428	0.9861
B2	0.9812	0.9926	0.0367	0.0232	0.9812	0.9925
B3	0.9493	0.9918	0.0367	0.0147	0.9492	0.9918
B4	0.9439	0.9891	0.0418	0.0184	0.9438	0.9890

Accurate state estimation and prediction not only rely on a precise model but also depend on the adjustments of model parameters to track the variation in the capacity fade. Gradually estimated parameters value converges to their respective actual values when more capacity data become available. Dynamic capacity fade characterization and estimation of current capacity for prediction of RUL are performed by using adaptive filter algorithm. Adaptive filter algorithm solves any estimation problem by minimizing the mean-square-error of discrete state space model.

The discrete state space model to describe the dynamic behavior of capacity fading, including the state transition and measurement equations can be expressed as follow:

TABLE 3.2: Parameters values for polynomial and exponential model

Battery	Parameter	Lower Bound	Mean	Upper Bound	Parameter	Lower Bound	Mean	Upper Bound
B1	p_1	-1.39E-06	-1.33E-06	-1.28E-06	e_1	-1.83E-03	-1.41E-03	-9.96E-04
	p_2	3.94E-04	4.41E-04	4.88E-04	e_2	7.07E-03	7.42E-03	7.77E-03
	p_3	1.00E+00	1.01E+00	1.02E+00	e_3	1.06E+00	1.06E+00	1.07E+00
B2	p_1	-1.59E-06	-1.55E-06	-1.52E-06	e_1	-4.69E-02	-3.78E-02	-2.87E-02
	p_2	4.62E-04	4.98E-04	5.34E-04	e_2	3.39E-03	3.61E-03	3.82E-03
	p_3	1.03E+00	1.04E+00	1.04E+00	e_3	1.12E+00	1.13E+00	1.14E+00
B3	p_1	-1.05E-06	-1.01E-06	-9.71E-07	e_1	-7.59E-04	-6.15E-04	-4.71E-04
	p_2	2.72E-04	3.11E-04	3.49E-04	e_2	7.34E-03	7.60E-03	7.86E-03
	p_3	1.01E+00	1.02E+00	1.02E+00	e_3	1.06E+00	1.07E+00	1.07E+00
B4	p_1	-1.28E-06	-1.24E-06	-1.19E-06	e_1	-2.08E-03	-1.68E-03	-1.27E-03
	p_2	4.32E-04	4.75E-04	5.19E-04	e_2	6.43E-03	6.69E-03	6.95E-03
	p_3	9.86E-01	9.94E-01	1.00E+00	e_3	1.05E+00	1.05E+00	1.06E+00
					e_4	-1.68E-04	-1.50E-04	-1.33E-04

State Equation

$$x_{k_c+1} = [e_{1,k_c+1}; e_{2,k_c+1}; e_{3,k_c+1}; e_{4,k_c+1}] \quad (3.7)$$

$$\begin{aligned} e_{1,k_c+1} &= e_{1,k_c} + \omega_{e1,k_c} \\ e_{2,k_c+1} &= e_{2,k_c} + \omega_{e2,k_c} \\ e_{3,k_c+1} &= e_{3,k_c} + \omega_{e3,k_c} \\ e_{4,k_c+1} &= e_{4,k_c} + \omega_{e4,k_c} \end{aligned} \quad (3.8)$$

Measurement Equation

$$Q_{k_c+1} = y_{k_c+1} = e_{1,k_c+1} * \exp(e_{2,k_c+1} * k) + e_{3,k_c} * \exp(e_{4,k_c+1} * k) + v_{k_c+1}$$

Where $w_{ei} \sim \mathcal{N}(\bar{w}_{ei}, \sum_{w,ei})$, $\sum_w, ei \in \mathbb{R}^{N_w, ei \times N_w, ei}$ and $v \sim \mathcal{N}(\bar{v}, \sum_v)$, $\sum_v \in \mathbb{R}^{N_v \times N_v}$ represents the process noise for each parameter and model measurement noise respectively. x_k refers parameters vector of capacity degradation model for cycle k and Q_k refers to measurement output which is battery capacity degradation data. With the measured capacity, the unscented Kalman filter is incorporated to adjust the parameters and update states value sequentially. In this process, predication of capacity is performed after the state value is updated. The RUL prediction is performed by the difference between predicated capacity cycle number and EUL cycle number:

$$RUL = k_{c,EUL} - k_{c,MC} \quad (3.9)$$

Where $k_{c,EUL}$ is the cycle number at which predicated capacity hits the capacity value at EUL point and $k_{c,MC}$ is the cycle number at which predication of RUL is performed.

3.3 Estimation Techniques

The adaptive filter algorithms estimate the needed state x_{k+1} based on the observations $y_{0:k+1} = [y_1, y_2 \dots y_k]$ under the rule of minimizing mean squared error between observation and estimated output [229]. The current state x_{k+1} recursively updates through predicted value of the previous state x_k . and current value of the measured input u_{k+1} . The state of a system is a group of dynamic variables that evolve through time, and its evolution through time is governed by a dynamic system, perturbed by process noise [230]. The measurements are functions of the state and the measurement noise. The basic idea of the

adaptive filter based techniques is the state space model, the system and measured signal combined with white noise.

3.3.1 Extended Kalman filter (EKF)

For estimation purpose, Kalman Filter (KF) was developed in 1960 [158]. KF is a linear filter the estimates states of the system by utilizing the measured value with noise and uncertainty and produces the value that approaches closer to the true value [49]. KF recursively updates the current state of the system through predicted value of the previous state and current value of the measured input. Since the battery is a non-linear system, linear KF cannot be utilized for SOC estimation purposes [164]. Hence to improve the estimation accuracy, the nonlinear version called the EKF used for SOC estimation of the battery. The EKF use Taylor-series to linearize the non-linear state equation and transform the nonlinear problem to linear problem.

To implement EKF, nonlinear state equation are linearizes about the current mean and the covariance using first-order Taylor-series expansion at each time step. Here assumption is made that both $f(\cdot)$ and $h(\cdot)$ are differentiable at all operating points,

$$f(x_k, w_k, u_k) \approx f(x_k, \bar{w}_k, \bar{u}_k) \quad (3.10)$$

$$\begin{aligned} \hat{A}_k &= \frac{df(\cdot)}{dx_k} \Big|_{x_k=\hat{x}_k^+} & \hat{B}_k &= \frac{df(\cdot)}{dw_k} \Big|_{w_k=\bar{w}_k} \\ \hat{C}_k &= \frac{dh(\cdot)}{dx_k} \Big|_{x_k=\hat{x}_k^-} & \hat{D}_k &= \frac{df(\cdot)}{dv_k} \Big|_{v_k=\bar{v}_k} \end{aligned} \quad (3.11)$$

Here, A_k represents $n \times n$ system matrix; B_k represents $n \times 1$ input matrix; C_k represent $m \times n$ output matrix; D_k is $m \times 1$ feed-forward matrix.

The detail computation process of EKF estimation strategies to develop an adaptive model-based internal states estimation is illustrated in Figure 3.3

Here, KG_k denotes the Kalman gain matrix, \hat{y}_k is the estimated measured output, \hat{x}_k^- and \hat{x}_k^+ are for the prior estimate before the measurement and the posterior estimate after the measurement respectively, $\Sigma_{x_k}^-$ and $\Sigma_{x_k}^+$ are covariance matrix of state estimation error before and after measurement respectively. In the multi-dimensional Taylor-series expansion, EKF obtained only first order accuracy in prediction of posterior mean and covariance of states. EKF does not take into account inherent uncertainty in prior states during the linearization process. In fact linearization around current state omits the

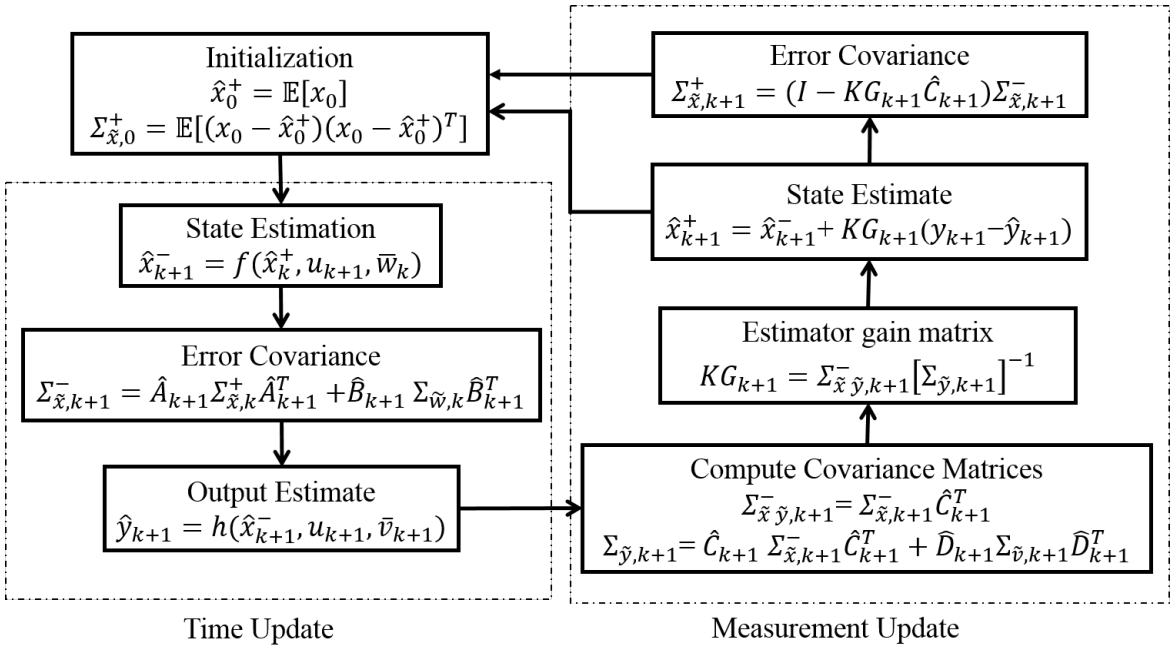


FIGURE 3.3: EKF algorithm based SOC estimation approach

crucial expectation operators. These approximations often introduce substantial error in evaluation of posterior mean and covariance of states which leads to divergence of the filter and suboptimal performance.

Disadvantages:

1. In the EKF, state distribution is propagated analytically through the first-order Taylor's series expansion. The first-order approximation introduce substantial errors in the prediction of posterior mean and covariance of states which leads to sub-optimal performance and sometimes divergence of the filter. Hence EKF is difficult to tune if model non-linearities are serve and leads to unreliable estimation of states.
2. EKF performance depends upon the accuracy of the system model and parameters. Even EKF performance will decrease or even diverge if the system and measurement noise don't satisfy the Gaussian distribution.

3.3.2 Sigma Points Kalman filter (SPKF)

EKF based estimation methods have some shortcoming which results in the decrease in the accuracy and leads to unstable filters. To overcome EKF shortcoming, SPKF utilizes small fixed group of function (called sigma points) to linearize the nonlinear system [165].

These sigma points are deterministically calculated using the mean and square-root decomposition of the covariance matrix of the prior state. Based on characterizing method, SPKF can be categorized as follow: Unscented Kalman Filter (UKF) and Central Difference Kalman Filter (CDKF). UKF utilizes the unscented transformation and CDKF utilizes Sterling's polynomial interpolation methods for linearization of the nonlinear system [231]. Using these approaches, if the dimension of the state is N_x then to capture first and second order moments of the prior states, $2N_x + 1$ sigma point χ_k are required with corresponding weights. Higher order moments can be captured, if so desired, at the cost of using more sigma-points. SPKF will eliminate the computational burden of Jacobian matrices and approximates up to second order. Hence, the calculation of derivatives could be avoided which implies that original function need not to be differentiable. The detail computation process of SPKF algorithmic is illustrated in Algorithm 3.4.

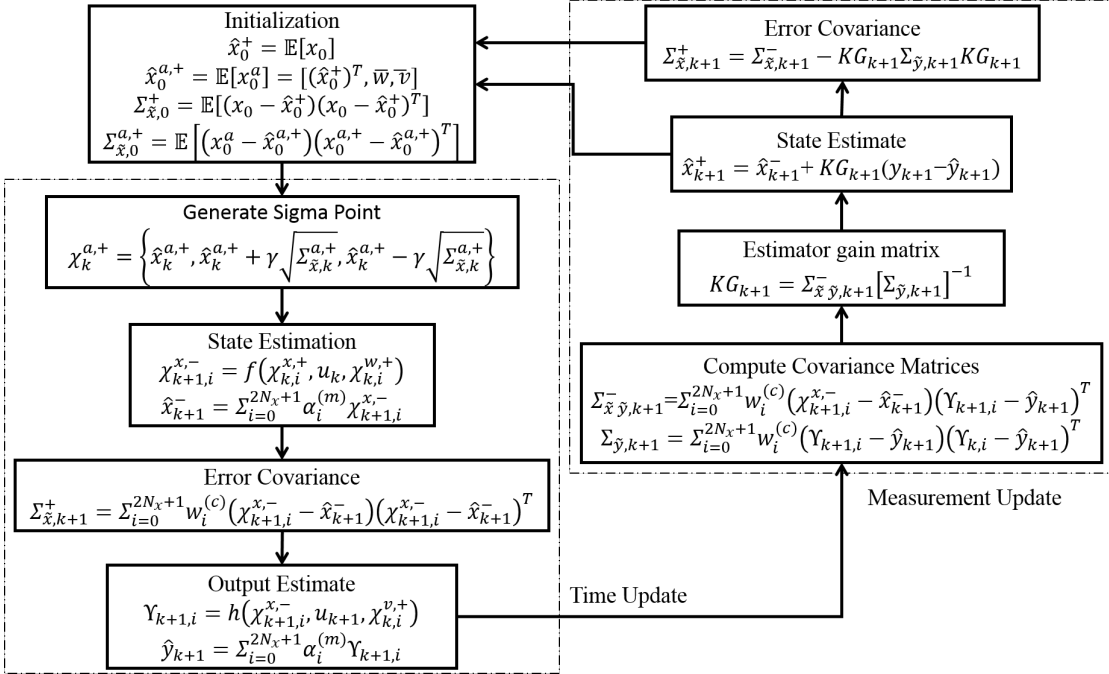


FIGURE 3.4: SPKF algorithm based SOC estimation approach

Here, γ is a scalar scaling factor that determines the spread of the sigma-points around the prior mean; x_k^a is the augmented random vector, $\hat{x}_{k-1}^{a,+}$ is posterior state estimate vector defined as $\hat{x}_{k-1}^{a,+} = [(\hat{x}_{k-1}^+)^T, \bar{w}, \bar{v}]^T$, $\Sigma_{\hat{x},k-1}^{a,+}$ is posterior covariance defined as $\Sigma_{\hat{x},k-1}^{a,+} = diag(\Sigma_{\hat{x},k-1}^{a,+}, \Sigma_{\bar{w}}, \Sigma_{\bar{v}})$, $w_i^{(m)}$ and $w_i^{(c)}$ are weighting constant. Both the filters follows same implementation procedure except the choice of sample points required more variable in case of UKF (α, β, κ) than CDKF (h). Weights are determined for both the filters has been shown in Table 3.3.

TABLE 3.3: Parameters values for different SPKF filters

Method	γ	$w_0^{(m)}$	$w_i^{(m)}$	$w_0^{(c)}$	$w_i^{(c)}$
UKF	$\sqrt{L + \lambda}$	$\frac{\lambda}{L+\lambda}$	$\frac{\lambda}{2(L+\lambda)}$	$\frac{\lambda}{L+\lambda} + (1 - \alpha^2 + \beta)$	$\frac{1}{2(L+\lambda)}$
CDKF	h	$\frac{h^2-L}{h^2}$	$\frac{1}{2h^2}$	$\frac{h^2-L}{h^2}$	$\frac{1}{2h^2}$

Here, $\lambda = \alpha^2(L + \kappa) - L$ with $10^{-2} \geq \alpha \geq 1$ and value of κ is either between 0 and 3-L. β incorporates prior information. h may take any positive value but optimal value is consider as $h = \sqrt{3}$ for Gaussian random variables.

3.3.3 Particle Filter (PF)

Accuracy of states estimation using EKF and SPKF depends on the accuracy of the model parameters. These filter also fails if used with nonlinear non Gaussian applications. Hence, to improve the robustness of estimation methods, Particle Filter (PF) was developed for dealing with complex distribution other Gaussian distribution. PF is a recursive statistical filter based on the Monte Carlo techniques and recursive Bayesian estimation. The Monte Carlo method is applied to approximate required state posterior probability distribution by a collection of random samples known as particles $x_{k=1}^{iN}$ with associated weight vector $w_{k=1}^{iN}$. Its complicated to draw random particles directly from the true posterior density function. Alternative and easy process to generate random particles is recursively update the posterior distribution using sequential importance sampling and re-sampling.

The PF algorithm is described as follows:

1. **Initialization:** Randomly draw N_p initial state particles $x_0^i (i = 1, 2, \dots, N_p)$ from prior probability distribution $p(x_0)$ having $\mathcal{N}(\bar{x}, \sum_x)$ and initial weight for particular particles is assigned as $w_0^i = 1/N_p$. Large the N_p the better the estimation but more computation will be needed. Number of particles N_p depend upon type of system and computation cost. The threshold of re-sampling can be initialized as $N_{th} = \frac{2}{3}N_p$.
For k=1,2,...
2. **Importance sampling:** Update the value of states using state equation and update the weight of the particle according to following equation:

$$w_{k+1}^i = w_k^i \frac{p(y_{k+1}|x_{k+1}^i)p(x_{k+1}^i|x_k^i)}{q(x_{k+1}^i|x_k^i y_{1:k})} \quad (3.12)$$

3. **Weight normalization** update and normalize the important weights for each particle. calculate the i^{th} particle's likelihoods.

$$w_{k+1}^i = \frac{w_{k+1}^i}{\sum_{i=1}^{N_p} w_{k+1}^i} \quad (3.13)$$

4. **Resampling:** Each particle is reserved or abandoned selectively according to its weight and then new set of particles is obtained.

$$N_{eff} = \frac{1}{\sum_{i=1}^{N_p} (w_{k+1}^i)^2} \quad (3.14)$$

If the effective sample size N_{eff} is below the given threshold N_{th} , then resampling procedure is performed to get the new particles.

5. **State estimation:** Using new set of N_p particles and their associated weights, propagates the state particles x_{k+1}^i to the next step by the system process equation.

$$\hat{x}_{k+1} = \sum_{i=1}^{N_p} \bar{w}_{k+1}^i x_{k+1}^i \quad (3.15)$$

3.4 Results and discussions

The high power Li-ion batteries (*LFP*) with a nominal capacity of 3.3 Ah and nominal voltage 3.7 V of the 18650 cylinder type were used for evaluation of the accuracy of state estimation methods. Capacity and life-cycle tests were executed for collecting reference data for evaluating the efficiency of adaptive filters in the estimation of internal battery states such as SOC and SOH respectively.

3.4.1 SOC estimation

A proper SOC estimation technique should be applicable of functioning efficiently during different loading conditions. To simulate the dynamic performance of EVs battery for actual driving load, US Advanced Battery Consortium (USABC) designed standard load profiles. Driving cycles are standardized driving pattern defined as the test cycles applied for evaluation and comparison of different types of drivetrains regarding their efficiency and emissions. These are sequences of speed-time data points which represents the driving behavior and traffic conditions in a specific area. Dynamic stress test (DST) driving

cycle profile represents driving conditions for an urban city travel pattern. When battery discharges from being fully charged (at 3.6V) to fully discharged (at 2V), the process includes several cycles of the standard DST cycle. Figure 3.5 illustrates sequence cycles for current and voltage of conventional DST profile at room temperature (25°C). This sequential driving profile is utilized for performance analysis of state estimator

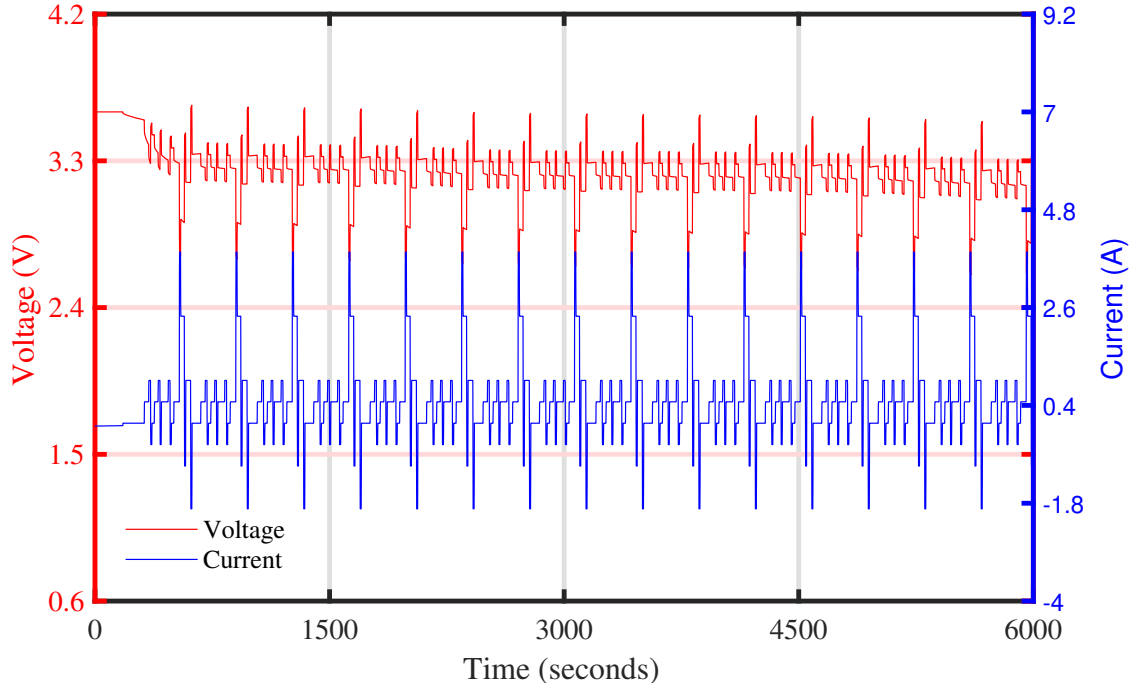


FIGURE 3.5: Voltage and current profile for DST driving cycles

Performance evaluation of different SOC estimation techniques is carried out with the different initial guess for the battery SOC. First, SOC estimation performed with assuming correct initial SOC value $\hat{x}_0^+ = [100]^T$ then assuming wrong initial SOC value $\hat{x}_0^+ = [90]^T$. Covariance of error was assumed as $\sum_{\tilde{x},k,0}^+ = \text{diag}([1e^{-3}])$. For the execution of estimation of SOC using EKF, UKF, CDKF, and PF, the value of the process \sum_p and observation \sum_m noise covariance were deliberately selected by using the trial-and-error method to assure convergence of the algorithms. For evaluation purpose white noise is assumed hence the mean value of process and measurement noise are set to be zero, and the value for the covariance of process noise \sum_p and measurement noise \sum_m are set to be 0.2. Particles for PF are assumed to be 200, and the threshold value for re-sampling is 0.5.

The required current value for the typical driving cycle is applied to the battery terminal in the laboratory, for simulating its dynamic discharge behavior during operation of EVs. In this dissertation, DST driving profiles are considered for evaluating the performance of adaptive filters methods for estimation of the battery SOC at different ambient

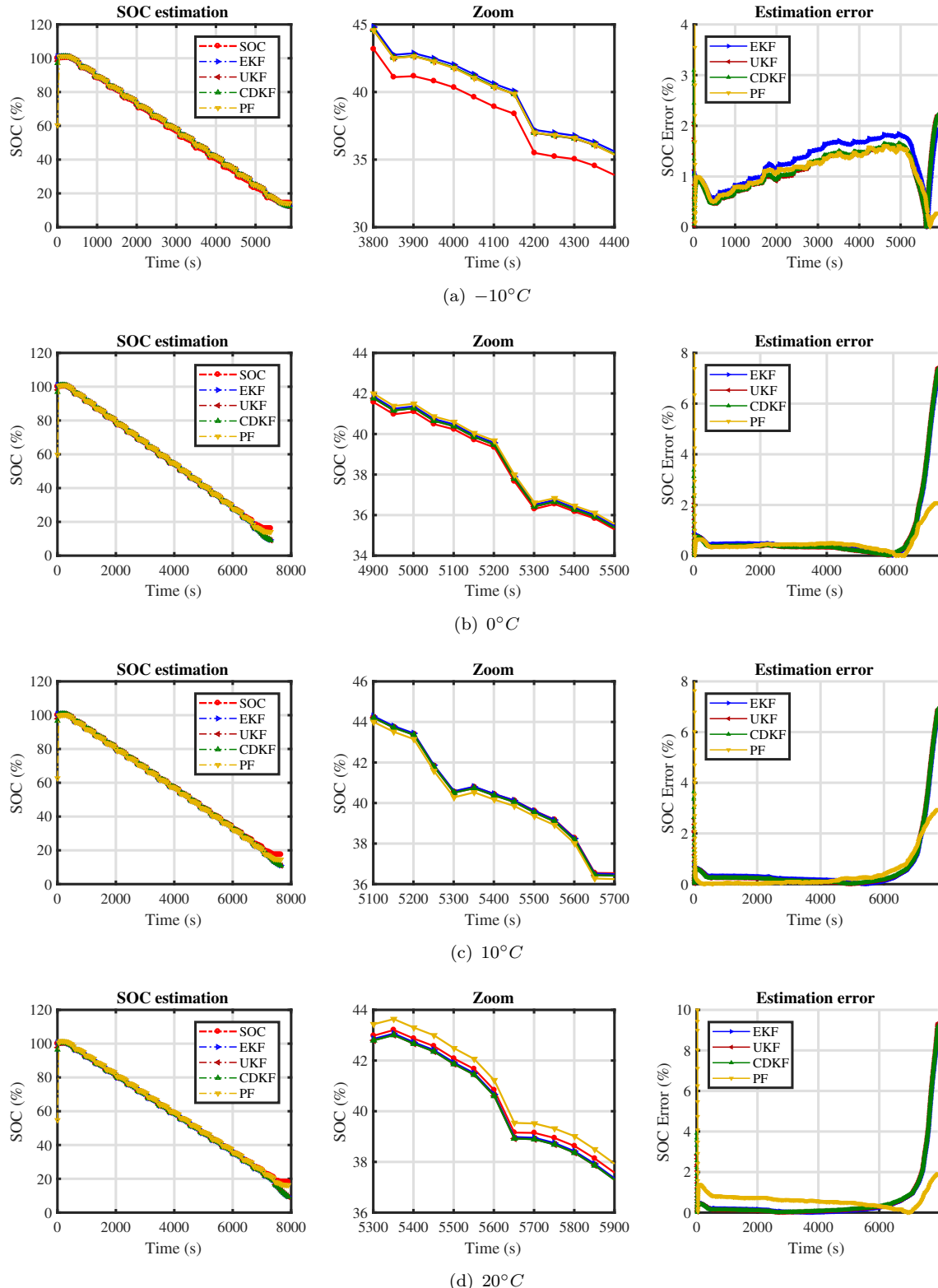


FIGURE 3.6: Estimation results of different adaptive KF assuming correct initial SOC value (a) -10°C (b) 0°C (c) 10°C (d) 20°C

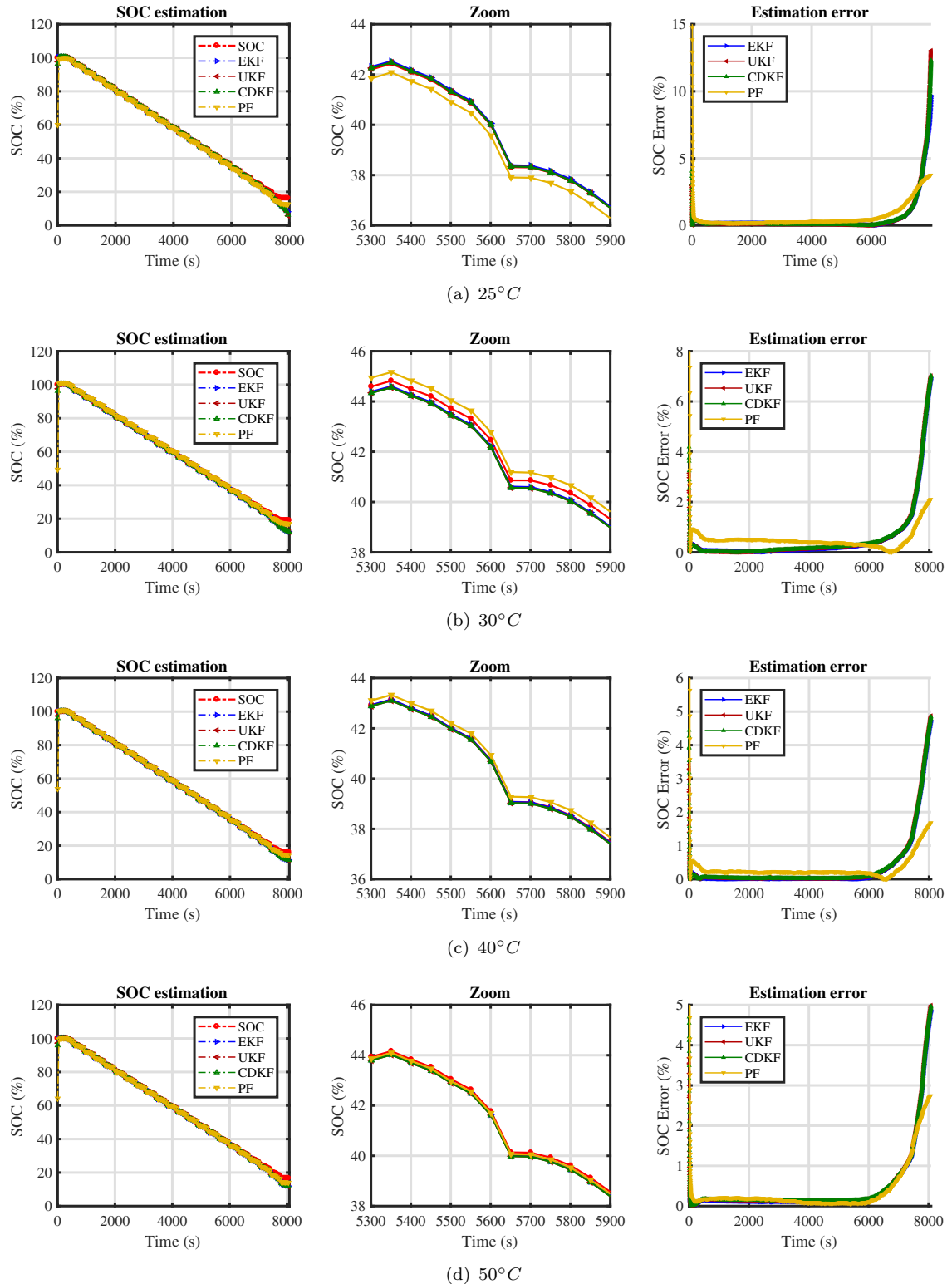


FIGURE 3.7: Estimation results of different adaptive KF assuming correct initial SOC value (a) 25°C (b) 30°C (c) 40°C (d) 50°C

temperatures. DST profile contains both processes discharging and charging with positive current defining discharge and negative current defining charge behavior of battery. Figure 3.6 and 3.7 illustrates recorded capacity test data using controlled ampere-hour method corresponding to the discharge of battery at different temperatures. In practical application usually, batteries are operated in between 20% to 90% SOC values only hence for estimation purpose data below 20% SOC is discarded.

Estimated SOC values with defining correct SOC initial value from adaptive filters at various temperatures is illustrated in Figure 3.6 and 3.7. The red color graph represents the true SOC value, while blue, brown, green and yellow graph represents the estimated SOC value using EKF, UKF, CDKF, and PF filters. Figure 3.6 and 3.7 contains SOC estimation values, zoom of SOC estimation graph and their errors in the estimated value for different temperatures. It can be observed from graphs that the estimated SOC value with correct initial SOC can track the true experimental SOC profiles more precisely with EKF and PF. Maximum absolute SOC error value is 2% , 8% , 8% , 10% , 15% , 8% , 6% and 5% ,and 5% corresponding to $-10^{\circ}C$, $0^{\circ}C$, $10^{\circ}C$, $20^{\circ}C$, $25^{\circ}C$, $30^{\circ}C$, $40^{\circ}C$ and $50^{\circ}C$ respectively for EKF, UKF and CDKF estimation methods. Whereas for all the temperature maximum absolute SOC error is approximately less 4% in case PF estimation. Hence, SOC estimation based on PF yields comparatively minor fluctuations. Error plots also indicate that corresponding to the low value of SOC estimated SOC slowly diverges away from reference SOC. The reason for large the difference between the values of SOC at the end of the graph is the error in the measurement of quantities using sensors and error due to Coulombic counting methods. Also, it's illustrated by figures that as the temperature value decreases battery discharges very fast compare to high-temperature value. Since SOC of the battery is less than 10% at $-10^{\circ}C$ whereas for another case its approximately more than 20%. Hence, the performance of the battery decrease with a decrease in the value of temperature. Hence a more accurate model to capture the transient behavior of the battery at low temperature is worthy to investigate in the future study.

Further quantification of estimators performance can be executed by determining root-mean-square and mean absolute error between reference SOC value and estimated SOC values. Mathematical, the root- mean- square error can be expresses by following equation:

$$RMSE = \sqrt{\frac{\sum_{k=1}^n (SOC_k^M - SOC_k^E)^2}{n}} \quad (3.16)$$

Mathematically, mean absolute error can be expressed by the following equation:

$$MAE = \frac{1}{n} \sum_{k=1}^n |SOC_k^M - SOC_k^E| \quad (3.17)$$

Here, SOC_k^M stands for measured SOC value from Coulomb Counting method and SOC_k^E stands for estimated SOC values from EKF, UKF, CDKF, and PF.

TABLE 3.4: Prediction error statistics at different temperature assuming correct initial SOC value

	RMSE				MAE			
	EKF	UKF	CDKF	PF	EKF	UKF	CDKF	PF
-10°C	1.3624	1.1917	1.2058	2.0506	1.2983	1.1265	1.1392	1.1957
0°C	1.3701	1.4033	1.4014	1.5598	0.7186	0.6740	0.6747	0.5744
10°C	1.2276	1.2569	1.2592	1.6133	0.5538	0.5299	0.5314	0.4732
20°C	1.4789	1.5253	1.5227	1.8996	0.5619	0.5796	0.5805	0.7218
25°C	1.3627	1.5524	1.5094	1.6596	0.5152	0.5196	0.5132	0.6946
30°C	1.2728	1.2947	1.2983	1.9615	0.5253	0.5488	0.5508	0.5994
40°C	0.9012	0.9267	0.9287	1.5579	0.3243	0.3530	0.3539	0.3828
50°C	0.9418	0.9669	0.9693	1.5062	0.4167	0.4561	0.4575	0.4431

TABLE 3.5: Execution time analysis (in secs) assuming correct initial SOC value

	EKF	UKF	CDKF	PF
-10°C	2.3757	2.2658	3.1938	1.9929
0°C	2.4426	2.3230	2.9864	2.0949
10°C	2.6293	2.8861	3.6077	2.5205
20°C	2.8277	2.5136	3.2501	2.5311
25°C	3.1270	2.5391	3.1446	2.6841
30°C	2.6307	2.5017	3.1987	2.2129
40°C	2.7071	3.1231	3.1356	2.2897
50°C	3.1084	2.5453	3.1657	2.2599

The value of root-mean-square and mean absolute error for different estimator is given in Table 3.4. From the table, it can be concluded that maximum root-mean-square error among all temperature for EKF is 1.37%, UKF is 1.55%, CDKF is 1.52 %, and PF is 2.05%. Maximum mean absolute error among all temperature using EKF us 1.2 %, UKF is 1.2%, CDKF is 1.3%, and PF is 1.19 %. Hence, the precision of EKF based estimation algorithm is higher than other algorithms for estimation of SOC at different temperatures. The execution time of the estimation methods is determined using "tic-toc" command in MATLAB to evaluate calculation time required to run the script. The execution time for performing battery SOC estimation is shown in Table 3.5. From the table, it can be concluded that the maximum execution time taken by EKF is 3.12 sec, UKF is 3.1 sec,

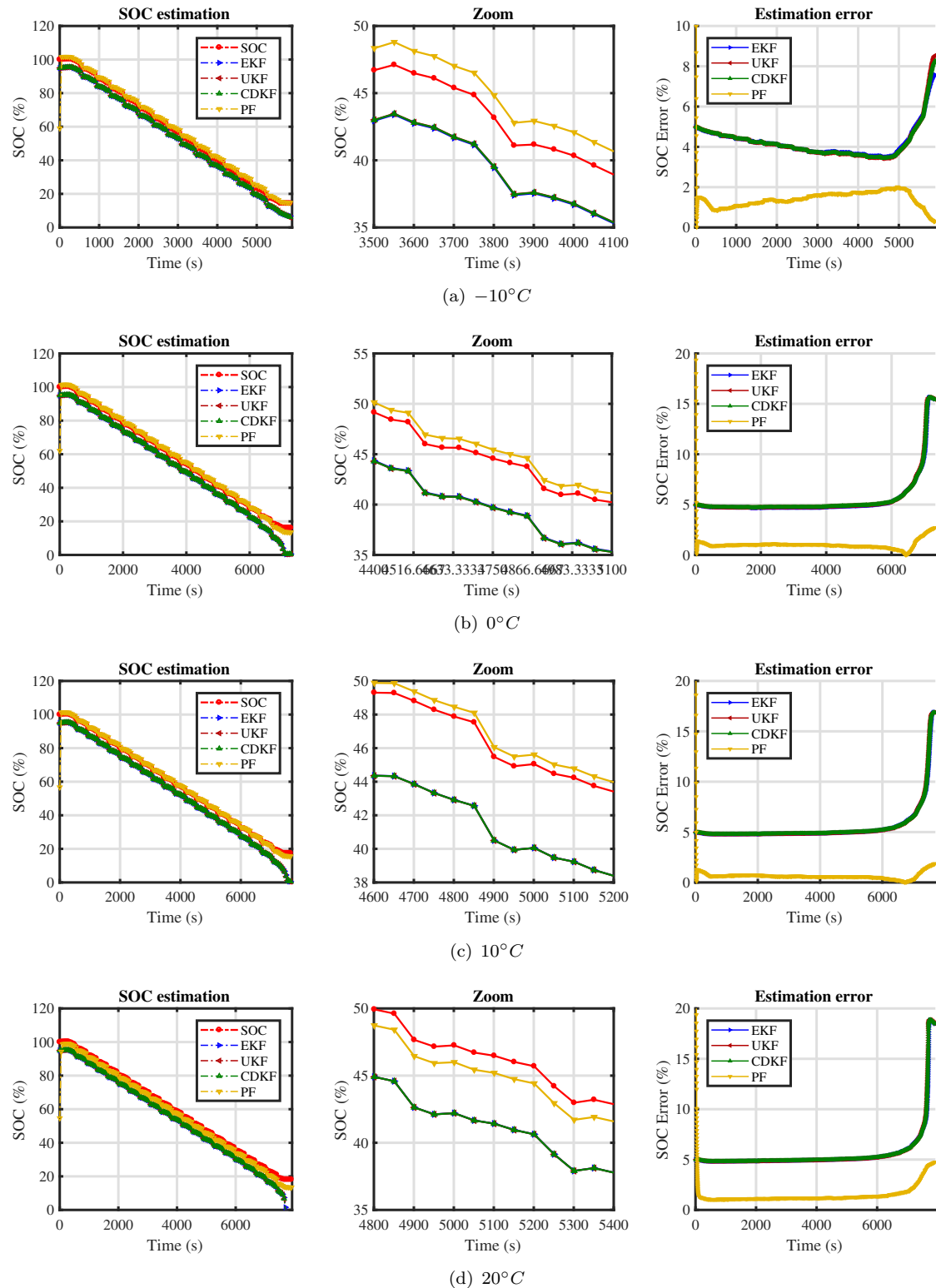


FIGURE 3.8: Estimation results of different adaptive KF assuming incorrect initial SOC value (a) -10°C (b) 0°C (c) 10°C (d) 20°C

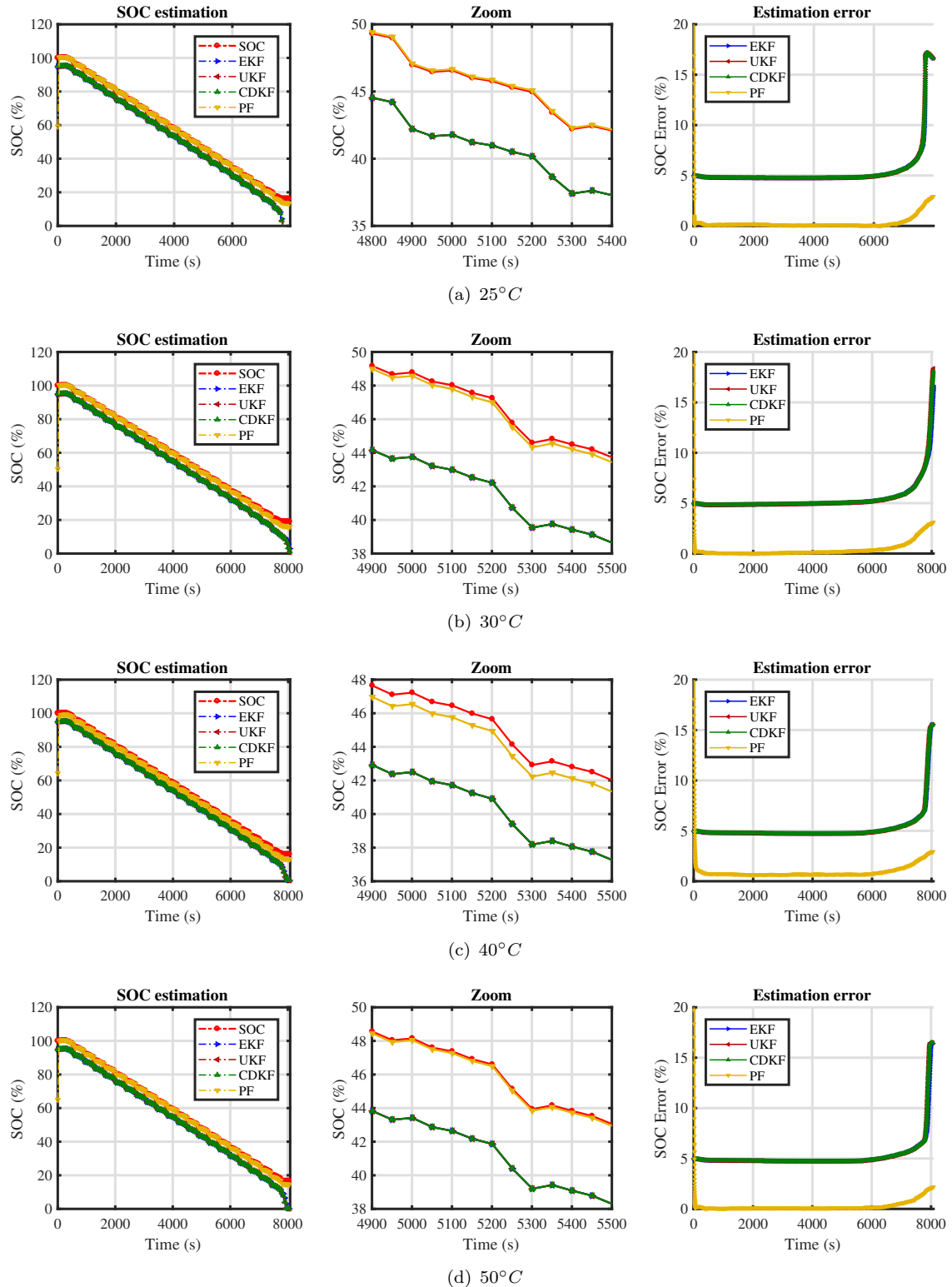


FIGURE 3.9: Estimation results of different adaptive KF assuming incorrect initial SOC value (a) 25°C (b) 30°C (c) 40°C (d) 50°C

SPKF is 3.6 sec and PF is 2.5 sec. Hence although the PF takes more computation cost, it is more robust than EKF to measure noise in the battery system.

The main drawback of Coulomb Counting method is that it depends upon initial SOC values in the estimation of current battery SOC value. If the initial values identification is not correct then estimated SOC values are not accurate. To identify the accuracy and efficiency of SOC estimation methods the effect of the incorrect initial SOC values is evaluated in this work. Estimated SOC values assuming incorrect SOC initial value from adaptive filters at various temperatures is illustrated in Figure 3.8 and 3.9. Similar to correct initial SOC values, the red color graph represents the true SOC value, while blue, brown, green and yellow graph represent the estimated SOC value using EKF, UKF, CDKF, and PF filters. Figure 3.8 and 3.9 contains SOC estimation values, zoom of SOC estimation graph and their errors in the estimated value for different temperatures. It can be observed from graphs that the estimated SOC value with incorrect initial SOC can track the true experimental SOC profiles more precisely PF. Maximum absolute SOC error value is 9% , 15% , 17% , 20% , 17% , 18% , 16% and 15% corresponding to $-10^{\circ}C$, $0^{\circ}C$, $10^{\circ}C$, $20^{\circ}C$, $25^{\circ}C$, $30^{\circ}C$, $40^{\circ}C$ and $50^{\circ}C$ respectively for EKF, UKF and CDKF estimation methods. Whereas for all the temperature maximum absolute SOC error is approximately less 4% in case PF estimation. Hence, SOC estimation based on PF yields accurate estimation of SOC for both correct and incorrect assumption of initial SOC values. The accuracy of other estimator decreases with the incorrect assumption of initial SOC values.

TABLE 3.6: Prediction error statistics at different temperature assuming incorrect initial SOC value

	RMSE				MAE			
	EKF	UKF	CDKF	PF	EKF	UKF	CDKF	PF
$-10^{\circ}C$	4.3076	4.3106	4.3058	2.0533	4.2392	4.2216	4.2238	1.4838
$0^{\circ}C$	5.9308	5.9890	5.9768	1.7938	5.5105	5.56106	5.5522	1.0995
$10^{\circ}C$	5.8593	5.8971	5.8864	1.7136	5.5108	5.5299	5.5248	0.7214
$20^{\circ}C$	6.1366	6.1799	6.1689	2.6904	5.6411	5.6630	5.6576	1.6184
$25^{\circ}C$	5.8978	5.9230	5.9154	1.3986	5.6411	5.6630	5.6576	1.6184
$30^{\circ}C$	5.5704	5.6820	5.6531	1.8870	5.4031	5.4492	5.4375	0.5012
$40^{\circ}C$	5.4584	5.4868	5.4786	1.7253	5.2189	5.2321	5.2281	1.0051
$50^{\circ}C$	5.4430	5.5418	5.5251	1.3590	5.2049	5.2504	5.2426	0.3365

The value of root-mean-square and mean absolute error for different estimator assuming incorrect initial SOC values are given in Table 3.6. From the table, it can be concluded that maximum root-mean-square error among all temperature for EKF is 6.13%, UKF is 6.17%,

CDKF is 6.16 %, and PF is 2.6%. Maximum mean absolute error among all temperature using EKF us 5.6 %, UKF is 5.66%, CDKF is 5.65%, and PF is 1.19 %. Hence, the precision of PF based estimation algorithm is higher than other algorithms as its execution doesn't depends on the initial values of SOC. The execution time for performing battery SOC estimation assuming incorrect initial SOC value is shown in Table 3.5. From the table, it can be concluded that the maximum execution time taken by EKF is 3.5 sec, UKF is 5.0 sec, SPKF is 3.9 sec and PF is 2.7 sec. This demonstrates that the PF can estimate the battery SOC with higher accuracy in less execution time with begin effect with initial values of the battery SOC.

TABLE 3.7: Execution time analysis (in secs) assuming incorrect initial SOC value

	EKF	UKF	CDKF	PF
$-10^{\circ}C$	2.3756	5.0729	3.1253	1.9885
$0^{\circ}C$	2.5128	2.8560	3.1434	2.8249
$10^{\circ}C$	3.4919	2.4770	3.0679	2.9406
$20^{\circ}C$	2.6106	2.5814	3.8407	2.2680
$25^{\circ}C$	2.6827	2.6363	3.8939	2.5423
$30^{\circ}C$	2.9738	2.6230	3.2060	2.7540
$40^{\circ}C$	2.6809	2.6483	3.9108	2.3036
$50^{\circ}C$	2.6404	3.3102	3.4300	2.3752

3.4.2 SOH estimation

Performance of the adaptive filters estimation techniques for prediction of RUL is discussed in this section. Four different batteries with same capacity has been utilize for analysis of capacity degradation behavior and effectiveness of the different estimation methods. Experimental data collected using lifespan test and exponential model of capacity degradation model is utilized for estimation process. Figures 3.10, 3.11, 3.12 and 3.13 visualizes predicted capacity using the exponential model utilizing different training data sets with different estimation techniques for batteries B1-B4 on different prediction cycles. In these graphs the green line indicates measured capacity data using life cycle test. The vertical line in each graph refers to the end of training samples after which capacity prediction performed using adaptive filters. The horizontal line in each graph refers the battery performance endpoint (EUL). To investigate the prediction performance of the models three different prediction points are used. Predication points are defined as the cycle at which battery reaches 1/3, 1/2 and 2/3 of life cycle test data.

The prognostic results for battery B1 with 1/3 cycles ($k_c = 187$), 1/2 cycles ($k_c = 280$) and 2/3 cycles ($k_c = 373$) data point of life-cycle datasets are used to update the model

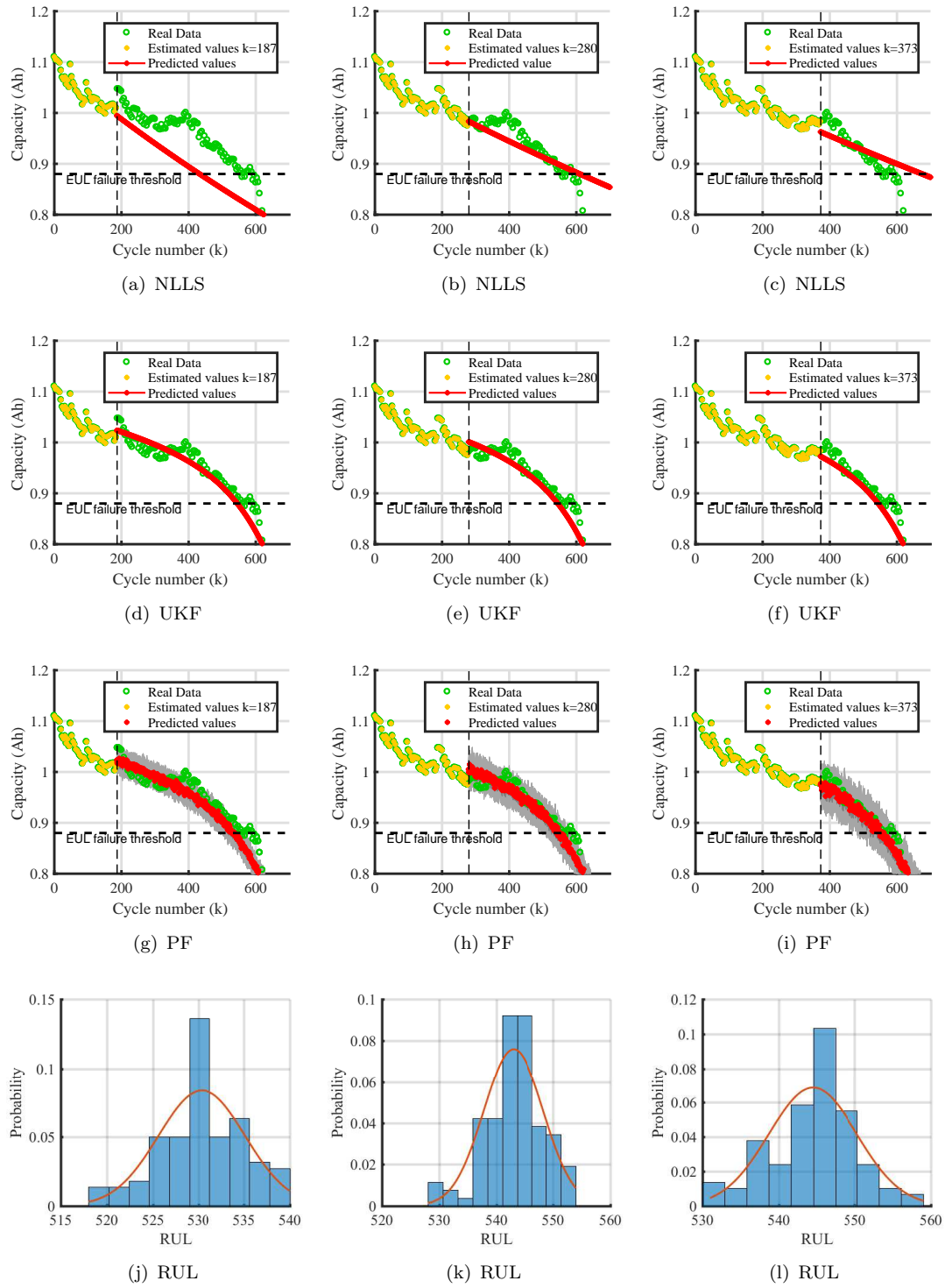


FIGURE 3.10: Comparison of RUL prediction results under different prediction point

using different estimation methods and probability distribution graph obtained from PF are shown in Figure 3.10 (a)-(d). Figure 3.10 (a) illustrate estimated capacity using NLLS

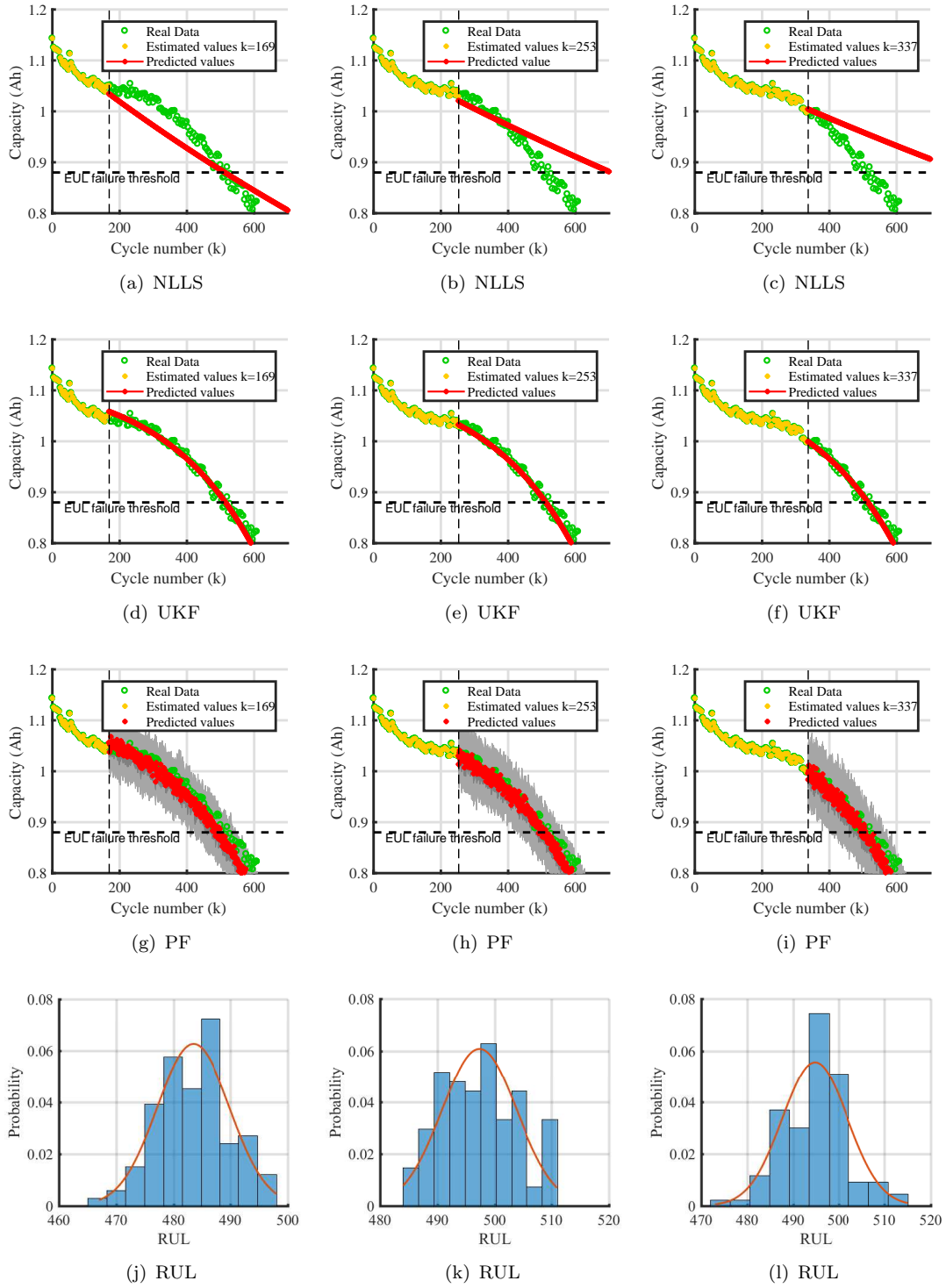


FIGURE 3.11: Comparison of RUL prediction results under different prediction point

with different training data sets. From graph it is concluded that with less training data sets NLLS provides very poor consistency in estimation. Where as with large training data

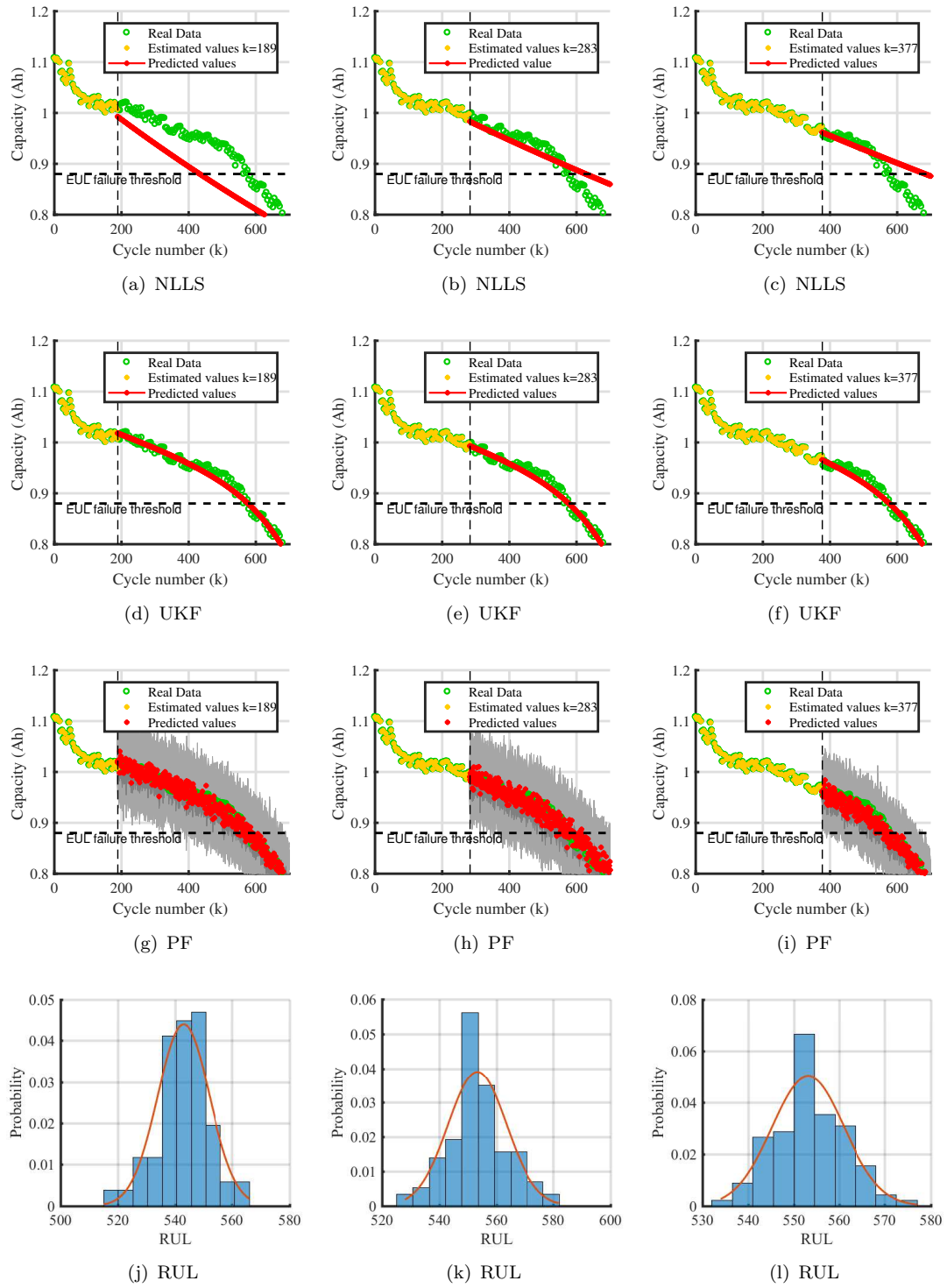


FIGURE 3.12: Comparison of RUL prediction results under different prediction point

also results are will poor as it can be seen through graphs that battery has been already reached to its EUL points where estimation still showing enough maximum capacity is

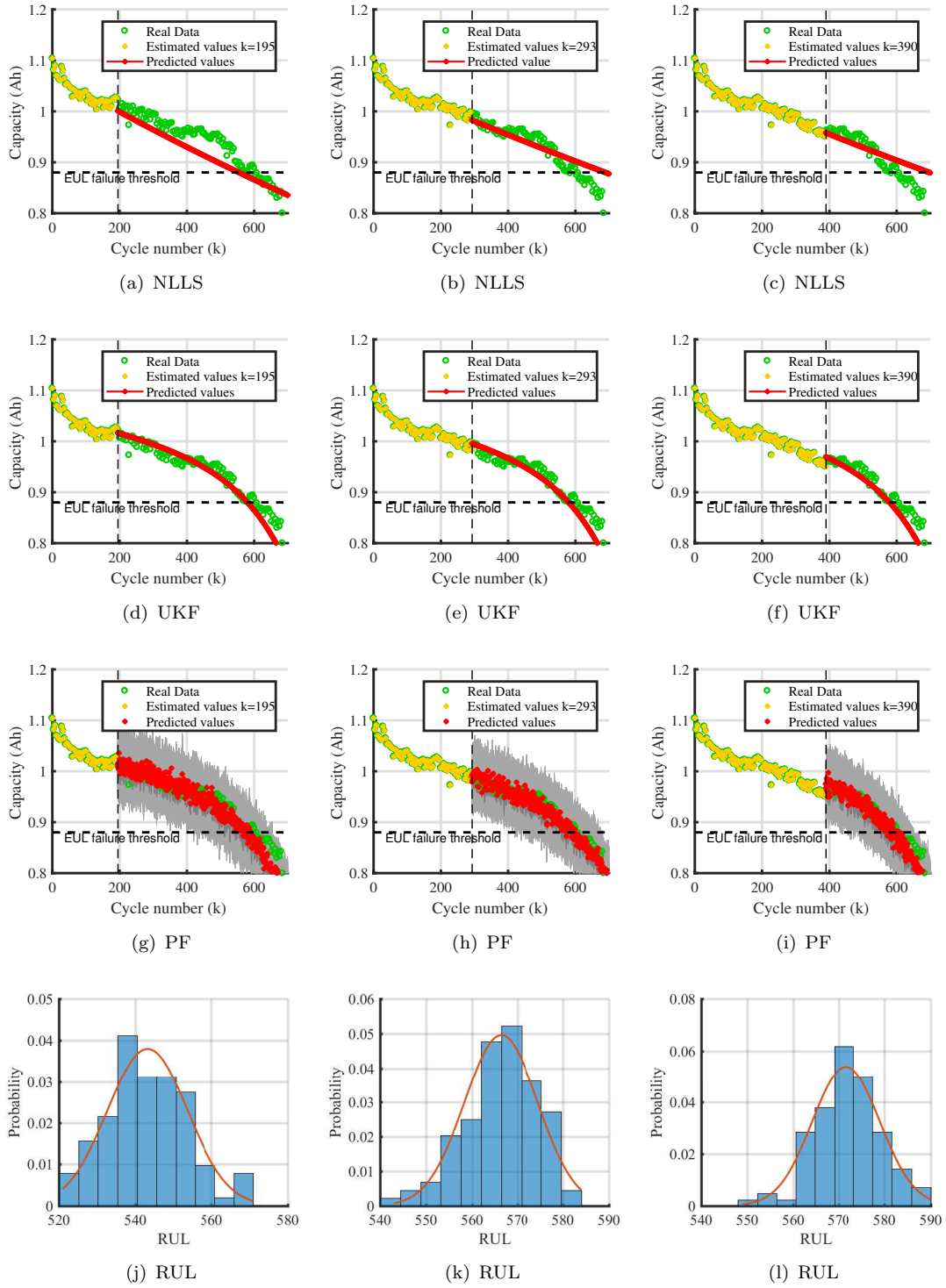


FIGURE 3.13: Comparison of RUL prediction results under different prediction point

available. Figure 3.10 (b) illustrate outcomes using UKF with different training data sets. From graph it is concluded UKF will provide approximately accurate estimation of

capacity. Similarly 3.10 (c) shows the distribution of particle for estimation of capacity and predicted capacity maximum capacity with each number of cycles with grey and red color respectively for different training data set. Advantage of particle filters is it provide more accurate estimation for all cycle values where as UKF diverted as from true capacity at some number of the cycles. Similarly Figure 3.11 shows prognostic results for the batteries B2 with the help of different data points of life-cycle test datasets for updating the model. Figure 3.11 (a) shows more clearly that NLLS is not appropriate for capacity estimation with all training data sets hence NLLS technique will be avoided for estimation of RUL of battery. Figure 3.11 (b) and (c) its clear that UKF and PF both are appropriate for estimation of battery maximum capacity with the variation of number of cycles. Figure 3.12 shows prognostic results for the batteries B3 with the help of different data points of life-cycle test datasets for updating the model. Different estimation methods are used are respective outcomes are shown in the graphs. Similarly prognostic results for B4 with different training datasets using NLLS , UKF and PF are shown in Figure 3.13. From all the analysis for capacity estimation for different batteries is concluded that UKF and PF provides accurate battery capacity estimation with the variations of number of cycles.

For analysis effectiveness of NLLS, UKF and PF in estimation of battery RUL comparison is shown in summarized in Table 3.8. Table contain information about actual failure cycle from datasets, prediction cycle, estimated failure cycle and prediction error. Actual failure cycle is the value of maximum battery capacity at EUL point for the capacity degradation data obtained from life-cycle test. Table show actual failure life for four batteries having same capacity and it can be seen that no two batteries will have same failure cycle number even they are manufactured identically because of variation in environmental conditions. Hence to identify SOH and RUL different of estimation are used. Prediction cycle is

TABLE 3.8: Performance comparison for RUL prediction using defined estimation methods

Battery ID	Real Failure cycle time	Prediction cycle (% cycle)	NLLS		UKF		PF	
			Cycle Number	Error	Cycle Number	Error	Cycle Number	Error
B1	560	187 (1/3)	434	126	546	14	533	27
		280 (1/2)	612	-52	546	14	546	14
		373 (2/3)	677	-117	545	15	551	9
B2	506	169 (1/3)	514	-8	516	-10	486	20
		253 (1/2)	708	-202	514	-8	492	14
		377 (2/3)	807	-301	516	-10	497	9
B3	566	189 (1/3)	435	131	578	-12	548	18
		283 (1/2)	629	-63	578	-12	542	24
		377 (2/3)	685	-119	578	-12	560	6
B4	585	195 (1/3)	556	29	581	4	568	17
		293 (1/2)	691	-106	581	4	574	11
		390 (2/3)	699	-114	580	5	574	11

value of cycle number at which estimation process for RUL is performed. Cycle at which battery reaches 1/3, 1/2 and 2/3 of life cycle test data are considered for calculating RUL at different cycle number. Prediction cycle values for different batteries are shown in the Table 3.8. Predicted RUL can be visualized as the cycle life from the end of the training sample till corresponding cycle at which battery capacity hits EUL line. Predication error is different between capacity values obtained from lifespan test and estimated capacity value at the EUL point. Predication error is shown in Table 3.8 having both value positive and negatives values. The positive error was showing that prediction on for battery EUL is before the actual occurrence of EUL whereas negative error showing that the prediction for EUL is after the actual EUL value. Early prediction of EUL will not affect battery, but prediction after EUL will cause catastrophic failures. It is concluded from Table 3.8 that predication error in case of NLLS and UKF are negative for most of cases hence NLLS and UKF are not suitable estimation techniques for prediction of RUL and SOH of the battery. Where as PF is having all positive value for predication error which shows that PF estimation battery failure way ahead hence replacement of battery can be performed by actually occurrence of it. PF particles probability distribution for prediction of RUL is assumed as Gaussian whose variance shown in Figure 3.10 (d), 3.11 (d), 3.12 (d) and 3.13 (d). This distribution is obtained from estimated values using by different particles in PF. For battery B1 estimation variance is 23 for 1/3 cycle , 24 for 1/2 cycle and 30 for 2/3 cycle data sets used for prediction. For battery B2 variances are 31 , 25 and 41 for training data set containing 1/3 cycle, 1/2 cycle and 2/3 cycle data points. Graph for probability distribution for battery B2 using PF is shown in Figure 3.11. Similarly of battery B3 and B4 probability distribution in prediction of RUL is shown in Figure 3.12 and 3.13 respectively for different training data points.

3.5 Chapter Summary

SOC estimation is the most significant function in battery management system which signifies residual range for recharge of battery and overcharge/overdischarge limit to enhance the life of battery. The contribution of this chapter is to systematically compare SOC based estimation strategies (EKF, UKF, CDKF and PF) in terms of SOC accuracy and individual advantages. Battery SOC for different operational conditions are identified and validated under DST driving cycle current profile. The comparison results confirmed at PF can be robust in practice as it provide the high estimation and prediction accuracy with the wrong initialized SOC values as well as correct initialized SOC. The results show that the PF can maintain simultaneously small errors and relatively fast computation time for real-time

applications compare to other non-linear filters. In addition, SOC estimation perform better at high temperatures than at low, hence a more accurate model to capture dynamics of battery at low temperature is worthy to investigate in future study. Battery aging leads to gradually deteriorates in battery capacity due to irreversible chemical changes while charging and discharging process. Degradation of battery capacity after threshold points causes insulation damage or catastrophic failures such as explosion and spontaneous combustion. In this chapter, two empirical model has been analyses for modeling battery capacity degradation over life-span of the battery. The exponential model inherently demonstrates the superiority in representing capacity degradation behavior compared to the polynomial model. Subsequently, the model has employed with NLLS, UKF and PF to deal with prediction of RUL of the battery. Three different datasets (1/3, 2/3 and 2/3 of the life cycle) are utilized for training, and remaining cycle datasets are utilized for prediction purpose. To address the uncertainties, a NLLS, UKF and PF approach was considered to adjust the model parameters and, hence, PF determined to be more accurate method to track the capacity fade. PF used state estimates from training data creating a diversity of particles. Adjustments were made to the weights of the particles, which affected the prediction PDF, but the state estimates were not changed from data available for predictions. The final RUL prediction can be obtained in the form of a probability density function so that the confidence level of the prediction can be assessed. Thus, the results demonstrate that PF provides the considerably accurate prediction of SOH and RUL with the less absolute error for different training datasets of all the batteries.